THE JOURNAL OF PHYSICAL CHEMISTRY C

Article

pubs.acs.org/JPCC

Quantum Efficiency Modification of Organic Fluorophores Using Gold Nanoparticles on DNA Origami Scaffolds

Suchetan Pal,[†,‡] Palash Dutta,[†,‡] Haining Wang,[§] Zhengtao Deng,[‡] Shengli Zou,[§] Hao Yan,[†,‡] and Yan Liu*[,†,‡]

[†]Department of Chemistry and Biochemistry and [‡]Center for Single Molecule Biophysics, The Biodesign Institute, Arizona State University, Tempe, Arizona 85287, United States

[§]Department of Chemistry, University of Central Florida, Orlando, Florida 32816, United States

Supporting Information

ABSTRACT: We used DNA origami as a platform to coassemble a 20 nm gold nanoparticle (AuNP) and an organic fluorophore (TAMRA) and studied the distance-dependent plasmonic interactions between the particle and the dye using steady state fluorescence and lifetime measurements. Greater fluorescence quenching was found at smaller dye-particle distances, which was accompanied by an enhancement of the decay rate. We also fabricated 20 and 30 nm AuNP homodimers using DNA origami scaffolds and positioned a Cy3 fluorophore between the AuNPs in both assemblies. For each particle size, three different interparticle distances were investigated. Up to 50% enhancement of the Cy3 fluorescence quantum efficiency was observed for the dye between the 30 nm AuNPs. These results are in good agreement with the theoretical simulations.

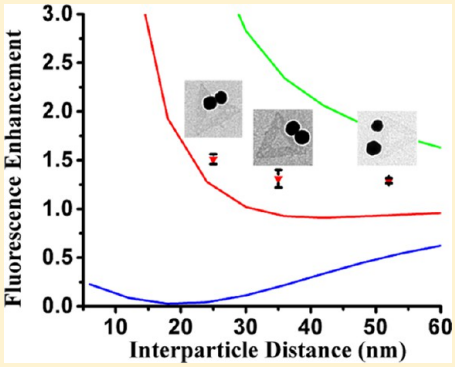

1. INTRODUCTION

DNA directed self-assembly has demonstrated itself as a robust and reliable way to organize nanomaterials into discrete, one-dimensional, two-dimensional, and three-dimensional architechtures.[1] In particular, DNA origami has emerged as a convenient method to form nanoscale structures with near-unity yields of formation, where the scaffolds display various functional moieties site-specifically placed on the surface with 4−6 nm spatial resolution. The most notable advantages of DNA origami platforms include the ability to organize discrete structures, their remarkably high yield of formation, their intrinsic structural rigidity, and the high density of modifiable DNA sequences that can be displayed from their surfaces.[2−4] Researchers have demonstrated the reliable organization of quantum dots, carbon nanotubes, virus capsids, proteins, enzymes, and aptamers on DNA origami scaffolds.[5−11]

Deterministic positioning of noble metal nanoparticles (NPs) using DNA origami[12−18] has attracted interest due to the unique distance and geometry-dependent optoelectronic properties of the NPs that can be studied.[19] For example, noble metal NPs are known to influence the quantum efficiencies and lifetimes of organic fluorophores in close proximity to the metallic particles. The considerable rigidity and structural predictability of double-stranded DNA (dsDNA) and DNA origami structures present an opportunity to use the structures as nanometer scale rulers and control the distance between photonic elements (e.g., NP−organic fluorophore or NP−NP). Recently, two groups reported the DNA-scaffolded organization of gold NPs (AuNPs) into chiral arrangements that gave rise to a unique response to circularly polarized light.[20,21] In addition, dsDNA was successfully used to systematically regulate the distance between fluorophores and metallic NPs.[22−24] Acuna et al. reported distance-dependent fluorescence quenching of organic fluorophores using DNA origami as a nanoscale molecular pegboard.[25] Highly modular DNA origami structures are the perfect platform for the systematic investigation of distance-dependent photonic interactions between NPs (of various sizes and noble metal compositions) and fluorophores. By selectively modifying DNA within the nanostructure, discrete NPs can be site-specifically immobilized, and precise nanogaps between particles can be engineered. Organic fluorophores can also be attached at specific positions, with the desired distance and orientation relative to the bound NPs.

In this study, diverse NP assemblies were created on a DNA origami platform to study the distance dependent local electric field enhancement of both monomeric and dimeric AuNP structures, as well as their effects on the photophysics of the fluorophores in close proximity to the AuNPs. These results are also compared with rigorous theoretical simulations.

2. METHODS

Materials. All unmodified staple strands were purchased from Integrated DNA Technologies Inc. (www.idtdna.com) in

Received: December 17, 2012
Revised: May 28, 2013
Published: May 29, 2013

   dx.doi.org/10.1021/jp312422n | J. Phys. Chem. C 2013, 117, 12735−12744

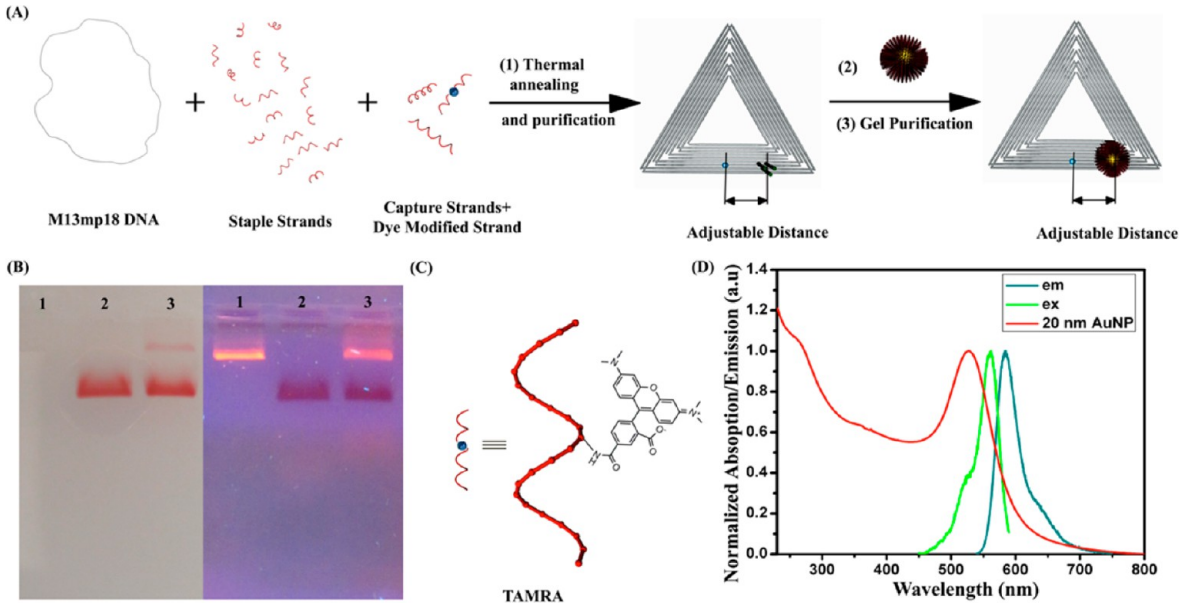

Figure 1. (A) Schematic representation of the formation of a triangular origami structure with a gold NP and a fluorophore molecule at predetermined positions. First, single-stranded M13 DNA, a collection of staple strands, selected capture strands that contain an extended probe sequence, and the fluorophore-modified strand were mixed at defined molar ratios and thermally annealed. Next the DNA origami structures are purified to remove excess single stranded DNA. The purified structures are subsequently mixed with DNA functionalized AuNPs, which hybrizide to the probe strands displayed from the DNA origami surface. Finally, the NP bound DNA origami structures are purified by native agarose gel electrophoresis to remove any free NPs. (B) White-light (left) and UV-light illuminated (right) native agarose gel images corresponding to purification steps. Lane 1: origami triangles. Lane 2: 20 nm DNA functionalized AuNPs. Lane 3: origami structures with a single 20 nm AuNP bound. (C) Molecular structure of a DNA strand with an internal TAMRA modification, where an *N*-hydroxysuccinimide ester (NHS-ester) is attached to an internal amine modified dT. (D) Excitation (green) and emission spectra (olive) of TAMRA on dsDNA plotted together with the AuNP plasmon band.

96-well plate format (normalized to 200 μM/well) and combined according to the various designs. All disulfide-functionalized DNA strands and fluorophore labeled strands were also purchased from IDTDNA and purified using denaturing polyacrylamide gel electrophoresis (PAGE) or high-performance liquid chromatography (HPLC). Tris-(carboxyethyl)phosphine hydrochloride (TCEP) and sodium chloride (NaCl) were purchased from Sigma-Aldrich, USA. Bis(*p*-sulfonatophenyl)phenylphosphine dihydrate dipotassium salt (BSPP) was purchased from Strem Chemicals, Inc. Colloidal solutions of 20 and 30 nm AuNPs were purchased from Ted Pella, Inc.

Phosphination of AuNPs. Prebound citrate ligands on the surface of AuNPs (20 and 30 nm) were replaced by BSPP ligands, in order to enhance the colloidal stability of the particles. Solid BSPP (20 mg for 20 nm particles or 30 mg for 30 nm particles) was added to a 50 mL solution of colloidal NPs (particle density of 7×10^{11}/mL for 20 nm NPs or 2×10^{11}/mL for 30 nm NPs provided by the manufacturer), and the mixture was stirred in the dark for 16–20 h at room temperature. Two to five milligrams of NaCl (solid) was added in increments to an agitated solution until the color changed from red to purple. The resulting solution was subjected to centrifugation (3000 rpm for 30 min), and the supernatant was carefully removed with a pipet to eliminate excess BSPP and NaCl. AuNPs were then resuspended in 1 mL BSPP (2.5 mM) solution. Two milliliters of methanol was added to the solution to aggregate the particles, and another centrifugation was used to remove any residual salt in the solution. The AuNP pellet was resuspended in 1 mL of 2.5 mM BSPP solution. The concentration of the AuNPs was estimated from the optical absorbance at ~520 nm using an extinction coefficient of 8.8×10^8 $M^{-1}cm^{-1}$ for the 20 nm particles and 6×10^9 $M^{-1}cm^{-1}$ for the 30 nm particles.[26] The phosphine coating increases the negative charge on the particle surface and consequently stabilizes the AuNPs in high salt concentrations.

DNA Functionalization of AuNPs. The disulfide bonds in the thiol-modified oligonucleotides were reduced to monothiol using TCEP (1:200 molar ratio of DNA:TCEP, overnight) in water. The oligonucleotides were purified using G-25 size exclusion columns (GE Healthcare) to remove the small molecules. The purified monothiol-modified oligonucleotides were incubated with phosphinated AuNPs in a 500:1 ratio for the 20 nm AuNPs and 1000:1 ratio for the 30 nm AuNPs in 0.5 × TBE buffer (44 mM Tris, 44 mM boric acid, 1 mM EDTA, pH 8.0). The NaCl concentration was gradually increased to 350 mM over 36 h at room temperature to ensure full coverage of the AuNPs by the thiolated DNA. The AuNP–DNA conjugates were washed 3 times using Microcon centrifugal devices (100 kD MWCO membrane filters, Millipore, Bedford, MA) in 0.5 × TAE-Mg^{2+} buffer (10 mM Tris, 5 mM Acetic acid, 0.5 mM EDTA and 6.25 mM Magnesium acetate, pH 8.0) to remove excess oligonucleotides and were finally resuspended in 0.5 × TAE-Mg^{2+} buffer. The concentration of these AuNP–DNA conjugates was estimated from the optical absorbance at ~520 nm using the previously mentioned extinction coefficients.

Formation of Origami Structures. To assemble the triangular shaped DNA origami, 3 nM single-stranded M13mp18 DNA (New England Biolabs, 7,249 nt length) was mixed in 0.5 × TAE-Mg^{2+} buffer with unpurified staple strands and selected capture strands (detailed sequence information is

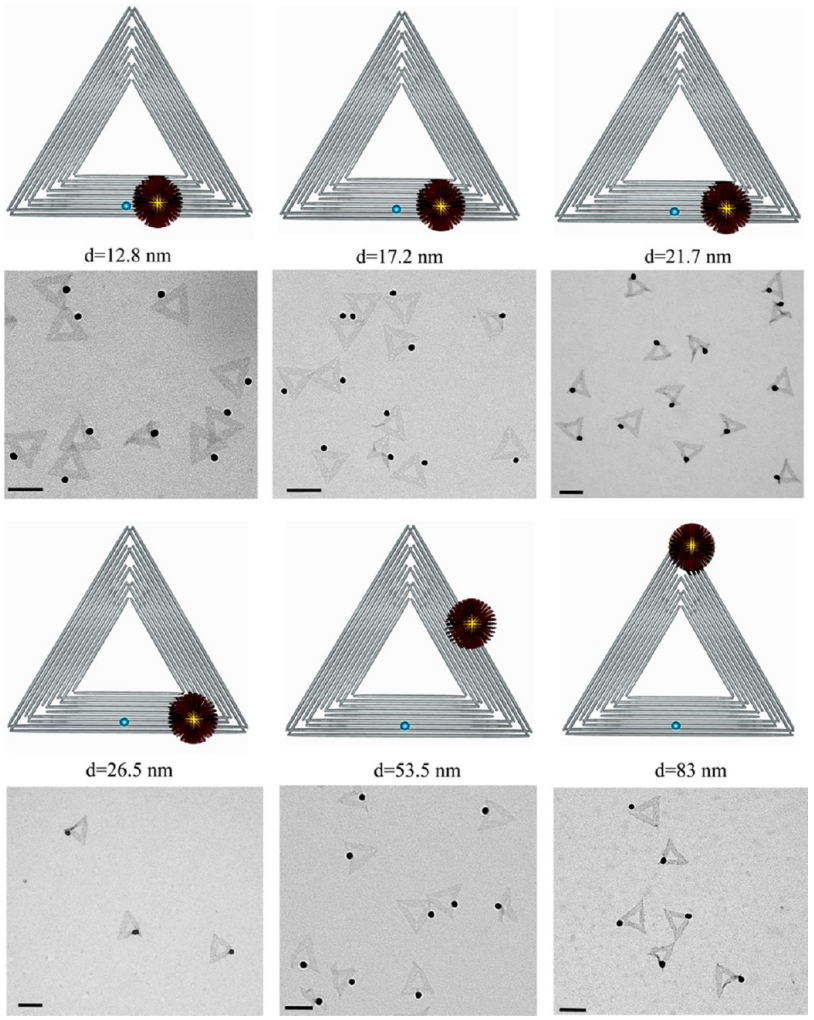

Figure 2. Schematic representations and corresponding negatively stained TEM images of monomeric constructs with different AuNP−dye distances. Nearly 100% yield of each construct is observed. Some distortions of the DNA origami scaffold are evident; these most likely resulted from imperfect deposition of the structures on the TEM grid, or exposure to vacuum conditions during TEM imaging which may cause the DNA structure to shrink. The scale bars are 100 nm.

shown in the Supporting Information (SI), Figures S31−42) in a 1:5:10 molar ratio. The resulting solution was cooled from 95 to 4 °C to form the DNA origami structure. The structures were subsequently purified three times by Microcon centrifugal filtration devices (100 kD MWCO filters, Millipore) to remove the excess staple strands.

Immobilization of AuNPs on DNA Origami and Electrophoretic Gel Purification. The DNA-functionalized NP solution was added to a 3 nM DNA origami solution (purified) in 0.5 × TAE-Mg^{2+}, with a molar ratio of 2:1 for the monomeric structures and 5:1 for the dimeric structures (2−2.5 fold excess of the AuNPs was added to ensure high yields of the desired structure). The concentration of NaCl was raised to 300 mM by adding 5 M NaCl solution. The mixture was then cycled 25 times between 45 and 30 °C in a polymerase chain reaction (PCR) thermocycler for 24 h to promote hybridization of the DNA on the AuNPs with the complementary capture strands on the DNA origami. The resulting mixture was subjected to 1% agarose gel electrophoresis for 40 min at a constant 80 V. The band containing the desired structure was excised from the gel, extracted using a Freeze 'N Squeeze column (Biorad) and concentrated by centrifugation at 6000 rpm for 10 min and finally redispersed in 0.5 × TAE-Mg^{2+} buffer. The samples obtained were used directly in the spectroscopic and transmission electron microscopy (TEM) characterizations. The gel purification gets rid of excess free AuNPs not associated with the DNA origami, and the extraction from the gel is mild enough not causing dissociation of the AuNPs from the DNA origami.

TEM Characterization of the Origami Triangles Functionalized with AuNPs. TEM samples were prepared by depositing 2 μL of the purified sample solution on a carbon-coated grid (400 mesh, Ted Pella) that was negative glow discharged using an Emitech K100X instrument. After 1 min, the sample drop was wicked from the grid by absorption into a filter paper. A drop of water was subsequently added to the grid to remove the excess salt, and the excess water was again wicked away by the filter paper. To stain DNA, the grid was treated with a drop of 0.7% uranyl formate solution for 2 s and the excess solution was wicked away with filter paper. The grid was then treated with a second drop of uranyl formate solution for 12 s, and the excess solution was removed by filter paper. Finally, the grid was kept at room temperature to allow drying. Staining permits the observation of the underlining DNA origami structure together with the AuNPs. TEM studies were conducted using a Philips

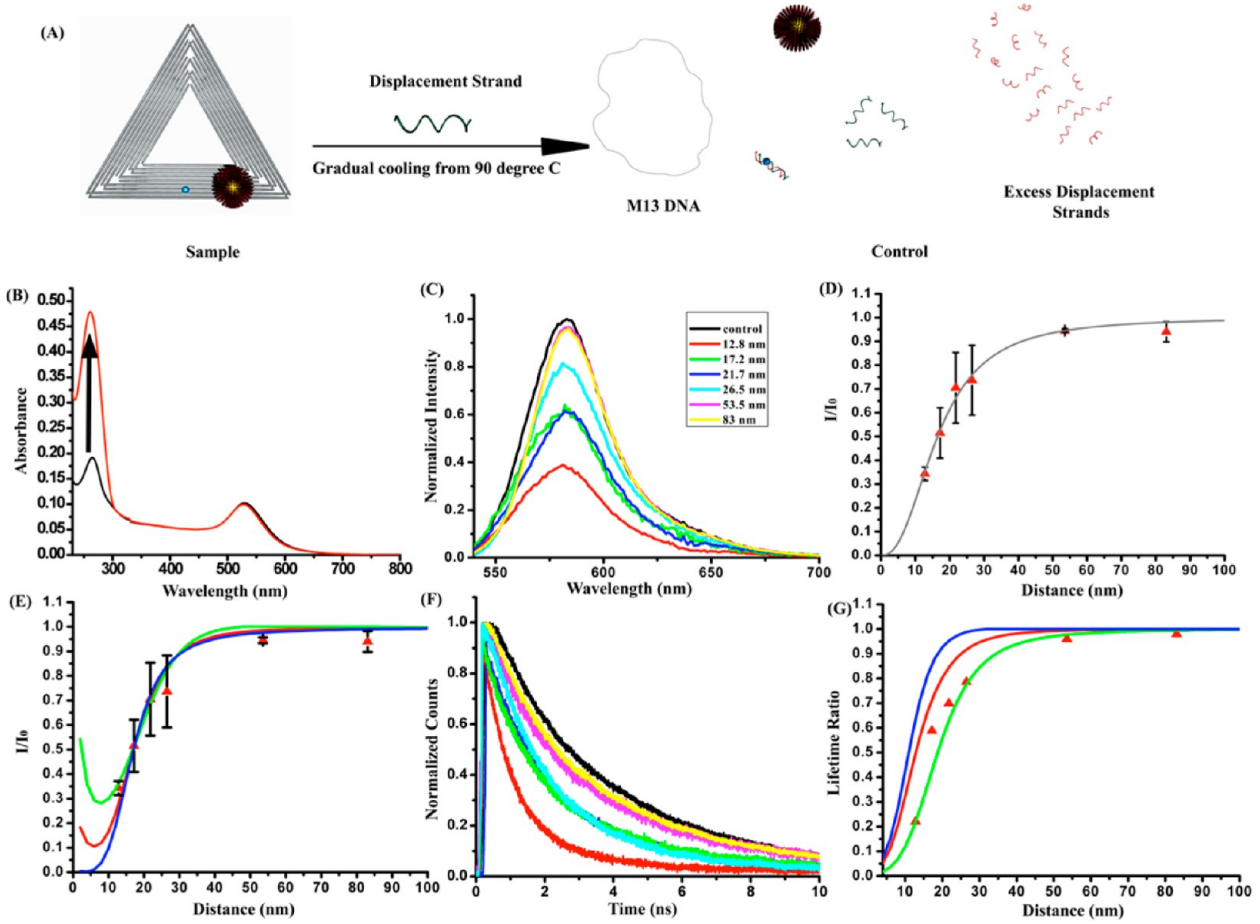

Figure 3. (A) Schematic representation of the sample with coassembled dye and monomeric AuNP at precisely controlled particle-fluorophore distance (left) and the corresponding control sample that contains exactly the same number of dye molecules and AuNPs but with a much larger average particle-fluorophore distance (right). (B) The UV–vis spectra of one representative sample (black) and the corresponding control (red). The absorbance at 260 nm (DNA) increases due to the addition of the excess displacement strand, but the absorbance peak at ~520 nm of the surface plasmons of the AuNPs remains unchanged. (C) The normalized emission spectra of different monomeric constructs of different particle–fluorophore distances, in which all the samples were excited at 525 nm. Control (black), 83 nm (yellow), 53.6 nm (pink), 26.5 nm (cyan), 21.7 nm (blue), 17.3 nm (green) and 12.8 nm (red). (D) The fluorescence intensity ratios of the assembled sample to the control at 580 nm for different fluorophore–AuNP distances (red triangles), plotted together with the corresponding curve fit using eq 1. (E) The same ratios are plotted with the theoretical predictions for different orientations of the fluorophores: average orientation (red), perpendicular orientation (green), and parallel orientation (blue) with respect to the particle surface. (F) Fluorescence lifetime decay curves for different particle-fluorophore distances, internally labeled (TAMRA) dsDNA with no AuNP (black), 83 nm (yellow), 53.6 nm (pink), 26.5 nm (cyan), 21.7 nm (blue), 17.3 nm (green) and 12.8 nm (red). (G) The ratio of the average fluorescence lifetime of the assembled sample to the control for different particle-fluorophore distances is plotted (red triangles) with the theoretical predictions for the different orientations of the fluorophores with respect to the particle: average orientation (red), perpendicular orientation (green), and parallel orientation (blue).

CM12 transmission electron microscope, operated at 80 kV in bright field mode.

3. RESULTS AND DISCUSSION

Fabrication of 1:1 Fluorophore–AuNP Constructs Using DNA Origami Directed Assembly. The assembly of DNA origami structures involves the combined action of ~200 short DNA staple strands to fold single-stranded genomic DNA (e.g., DNA of M13mp18) into geometrically well-defined nanopatterns that are fully addressable, with a spatial resolution determined by the distance between staple strands. Figure 1A illustrates how we coassembled an organic fluorophore and metal NPs at specific particle-fluorophore distances. Automated solid-state chemical synthesis of DNA enables incorporation of a fluorophore at any position within a single stranded DNA. For the experiments described here, we internally modified a selected DNA staple strand with a TAMRA fluorophore. The molecular structure of TAMRA is shown in Figure 1C. Internal dye modification of the staple strands ensures that the fluorophore molecules are fixed at specific locations on the origami surface. We also extended three staple strands (capture strands) by 15 nucleotides, complementary to the ssDNA displayed from the AuNPs, for site-specific immobilization of the AuNPs on the DNA origami platform, following Ding et al.[13] The position of the TAMRA molecule was fixed for all constructs, while the position of the three capture strands was adjusted to realize several particle-fluorophore distances. The overall fabrication process contained two steps: first, M13mp18 DNA, the fluorophore modified strand, and the staple strands (including the capture strands) were mixed, and the mixture was annealed from 90 to 25 °C over 12 h. The excess short DNA strands were removed using a Microcon centrifugal device (MWCO 100kD). In the second step, AuNPs were mixed with the purified DNA origami solution and then

dx.doi.org/10.1021/jp312422n | J. Phys. Chem. C 2013, 117, 12735–12744

subjected to another annealing step and native agarose gel purification. Figure 1B shows the white-light and UV-light illuminated image of a typical purification gel. The fastest bands in lanes 2 and 3 correspond to the free AuNPs; the second band in lane 3 corresponds to the desired AuNP monomeric structure on DNA origami. This particular band was excised and the DNA extracted to obtain the desired structures for further measurements.

The fluorophore we selected for these experiments has well-characterized photophysical properties. TAMRA exhibits an absorbance maximum at ∼559 nm and an emission maximum at ∼580 nm, and has a fluorescence lifetime of ∼2.8 ns in aqueous buffer. The optical properties of the TAMRA-modified single stranded DNA are shown in Figure 1D. No changes in the photophysical properties were observed when the strand was incorporated into DNA origami. The schematic drawings in Figure 2 illustrate the distances between the surface of the particle and the fluorophore that were investigated. The particle-fluorophore distances were calculated using the known dimensions of the triangular origami structure (114 nm for each arm) and the length of double stranded DNA (3.4 nm/10.5 base pairs) (see SI Figure S30 for a schematic illustration of the formula and geometric parameters used for the calculation). The corresponding TEM images shown in the lower panels of Figure 2 reveal efficient positioning of the 20 nm AuNPs at the predetermined positions, illustrating the successful formation of the desired structures (see SI Figures S1−S12 for additional zoom-out and zoom-in images). All of the constructs were formed with greater than ∼95% yield (see SI Table S1 for detailed yield statistics).

Note that the three capture strands displayed from the DNA origami surface are arranged in a triangle. If all three capture probes are fully hybridized to the corresponding three DNA strands on the same AuNP, then the AuNP should have little translational freedom, except for the flexibility provided by a 5-nt single stranded linker region between the hybridization domain and the underlining DNA origami structure. Thus, the uncertainty of the AuNP position relative to the position of the fluorophore is expected to be less than 1.5 nm. On the other hand, the distribution of diameters for the 20 nm AuNP, as determined from TEM images, is ∼2 nm. Therefore, the edge-to-edge distance between the particle and fluorophore is associated with a roughly 2 nm uncertainty.

Distance-Dependent Photonic Interaction of TAMRA and a Monomeric 20 nm AuNP. *(a). Steady State Measurements.* In order to verify the effect of NP, we created a system where the fluorophore is completely separated from the NP as a control experiment. The control samples were produced by adding ∼100 fold excess of ssDNA that is fully complementary to the fluorophore modified DNA, and subsequently heating the mixture to 80 °C followed by rapid cooling to room temperature. The process is schematically depicted in Figure 3A. The resulting dismantled structures were examined by TEM; there is no evidence of well-formed structures in the control samples (see SI Figure S26). The addition of displacement strands and the subsequent heating did not result in any change in the gold NP plasmon band, as shown in Figure 3B. Note that the addition of excess displacement strands and disruption of the DNA origami structures resulted in an increase in the DNA signature absorbance peak at 260 nm, as expected. The absorbance peak of the dye (only one dye per ∼7250 bp DNA origami) is too small to be observable, as the extinction coefficient of the dye (9.1×10^4 M^{-1} cm^{-1} for TAMRA) is ∼3−4 orders of magnitude smaller than that of the 20 nm AuNP. However, the concentration of the dye and AuNPs in the control sample remains the same. By measuring the fluorescence intensities of the fully assembled constructs and comparing the results to the corresponding control samples with the same optical density (OD) at the excitation wavelength, the steady state fluorescence intensities can be directly compared, and any observed differences will reveal the distance dependent plasmonic effects.

We collected the fluorescence emission spectra of each assembled sample and the corresponding control under the same experimental conditions (excitation at 525 nm). The normalized spectra (with respect to the corresponding control samples) are shown in Figure 3C. As the distance between AuNP and dye decreased, the intensity of dye emission decreased as well. To highlight this effect, we plot the ratio of the fluorescence intensities of the assembled samples to the control against the particle-fluorophore distance (Figure 3D). The ratios essentially reflect the level of fluorescence quenching of the dye due to the proximity of the AuNP, with greater quenching when the dye molecule and the particle are closer. The quenching effect is significant when the particles and dyes are 10−30 nm apart, and diminishes beyond ∼60 nm.

Förster resonance energy transfer (FRET) is commonly employed to describe the energy transfer between two fluorophores, which can be approximated as discrete dipoles. FRET occurs through electromagnetic coupling of two dipoles and the rate of energy transfer is shown to be proportional to $1/d^6$, where d is the distance between the dipoles.[27] FRET effects are detectable over very short distances and active up to 1−10 nm distances. Clearly, the interaction between a fluorophore and a AuNP is detectable at distances much greater than 10 nm and thus, cannot be modeled by a traditional FRET mechanism.[33,34] To address the interactions of dye molecules with NPs over distances greater 10 nm, nanosurface energy transfer (NSET) has been proposed.[23] Here, the quenching behavior is proportional to $1/d^n$, where d is the distance between the fluorophore and the NP surface; in addition, the index n is expected to be 4 in NSET, rather than 6 as in FRET. Here, the quenching (Q) vs interparticle distance was fit (gray plot in Figure 3D) by the equation

$$Q = 1 - \frac{1}{\left[1 + \left(\frac{d}{d_0}\right)^n\right]} \quad (1)$$

as reported previously,[22,23] where d_0 is the distance at which 50% quenching is observed. The d_0 and n values were found to be 16.5 ± 0.3 nm and 2.43 ± 0.06, respectively, for the 20 nm AuNP/fluorophore assembly. The value of n is significantly lower than the values obtained for small sized particles (5 and 10 nm AuNPs, in which n = 3.3−4.5 were observed).[22] This result confirms the long-range quenching behavior of larger particles, and the necessity to develop more rigorous theoretical models.

The quenching effect of AuNPs on fluorophore molecules can be modeled by a rigorous electrodynamic method developed by Zou et al.[22,28,29] In this theoretical modeling method, the fluorophore molecule is treated as a radiating dipole. When the molecule is situated close to an AuNP, the emitted fluorescence signal from the molecule may be amplified due to the enhanced local electric field near the metal NP, at

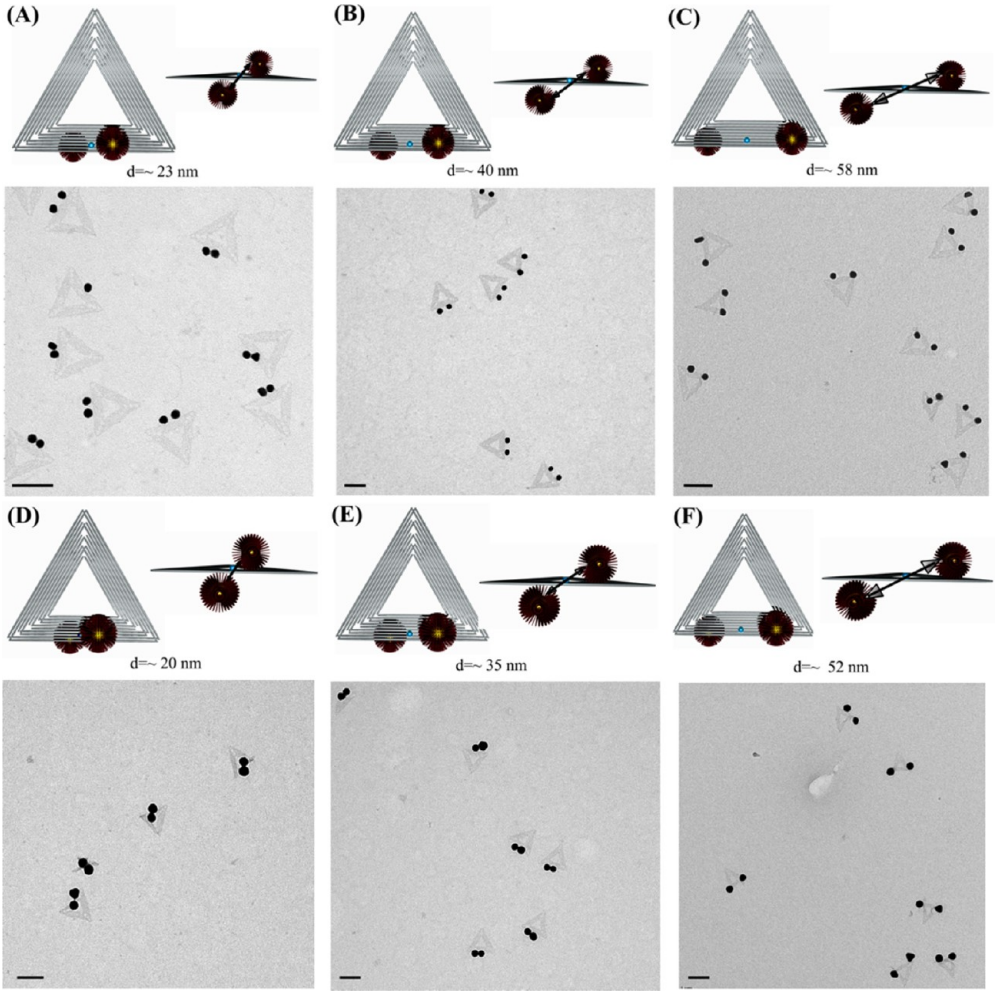

Figure 4. Schematic representations of the top and side views of each assembly and the corresponding negatively stained TEM images of the 20 nm dimeric constructs with three different interparticle distances (surface to surface): (A) 23, (B) 40, and (C) 58 nm, and 30 nm dimeric constructs with three different interparticle distances: (D) 20, (E) 35, and (F) 52 nm. Scale bar is 100 nm in all TEM images.

both the excitation wavelength and the emission wavelength. On the other hand, the signal will also be quenched due to the nonradiative energy transfer between the molecule and the metal NP at the emission wavelength. The measured fluorescence signal of the system, including a molecule and a metal NP, as compared to that of an isolated molecule, can be calculated by

$$f = f_{ex} \times f_r \times q_{em} \quad (2)$$

Where f_{ex} is the enhancement factor at the excitation wavelength, which is proportional to the enhanced local electric field, $|E|^2$, of the metal NP at the position of the molecule at the excitation wavelength; f_r is the enhancement factor at the emission wavelength, which is also proportional to the enhanced local electric field, $|E|^2$, at the emission wavelength; and q_{em} is the quenching factor due to the nonradiative energy transfer between the molecule and the metal NP at the emission wavelength. The q_{em} can be obtained by $1/(f_t \times \eta + 1 - \eta)$, where η is the quantum efficiency (QE) of an isolated fluorophore molecule, and f_t is the enhancement factor of the decay constant of the excited dye molecule, which includes the energy emitted (radiative) by the molecule and the metal NP, and absorbed (transferred and nonradiative) by the metal NP relative to the radiative constant of an isolated dye molecule. The electric field around the metal NP at different wavelengths (f_{ex} and f_r) was calculated using the Mie theory and averaged over different orientations. The coupling between the molecular dipole and the AuNPs is treated with the coupled dipole method.

The theoretical quenching curves for different orientations of the fluorophore with respect to the AuNP surface are plotted together with the experimental data points in Figure 3E. The data shown in Figure 3E is based on the theory that predicts the fluorescence intensity of the dye as a function of dye−particle distance (with different dye orientations with respect to the surface of the metal NP), which do not show significant differences except for at very close fluorophore−particle distances (<15 nm). All of the experimental data agrees very well with the theoretical predictions in the range of distances that were examined.

(b). Fluorescence Lifetime Measurements. The fluorescence lifetime of an excited state fluorophore is also influenced when a metal NP is in close proximity to the fluorophore. We used the time-correlated single photon counting technique (TCSPC) to measure the fluoresecence decay lifetimes of each assembled construct with various fluorophore-particle distances (Figure 3F). The TCSPC decay kinetics were analyzed with a home-written software package ASUFIT

dx.doi.org/10.1021/jp312422n | J. Phys. Chem. C 2013, 117, 12735−12744

(www.public.asu.edu/~laserweb/asufit/asufit.html) and fit by a sum of multiple exponential decay model according to

$$f(t) = \sum a_n \exp(-t/\tau_n) \quad (3)$$

where $f(t)$ is the measured experimental kinetic decay curve, a_n is the amplitude for the nth exponential component, and τ_n is the corresponding lifetime. Numerically averaged lifetimes were calculated according to eq 4. The fitting parameters are shown in SI Table S3.

$$\tau_{av} = \sum a_n \tau_n \quad (4)$$

As shown in Figure 3F, the decay becomes faster as the particle−dye distance decreases. In Figure 3G, the ratio of the average lifetime of the constructs to internally modified (TAMRA) dsDNA was plotted against the particle-dye distance and overlaid with the theoretically predicted lifetime ratios, revealing the distance dependence of the dye with various orientations (refer to the direction of the dipole moment of the dye with respect to surface of the NP). The experimental data is in fairly good agreement with the theoretical predictions, with all the experimental data in between the average and perpendicular orientations. It should be noted that the internally modified TAMRA within the DNA strand may be intercalated between neighboring base pairs (supported by high fluorescence anisotropy measurement ~0.28), thus the dye has a relatively fixed orientation. From this data we conclude that the dipole moment of the dye has an orientation more perpendicular than parallel to the surface of the particle. However, further structural investigation is needed to determine the absolute dye orientation.

Fabrication of Dimeric AuNP Structures with a Fluorophore in the Gap. Dimeric AuNP arrangements greatly enhance electric fields in the space between the particles (see Figure S25 for a comparison of the electric field enhancement of the dimer and monomer structures).[30] Recently, Busson et al. placed a single fluorophore in between two 36 nm AuNPs and demonstrated an accelerated single photon emission compared to the corresponding monomers.[31] The DNA origami method gives us the unique opportunity to adjust the nanogap by not only changing the interparticle distance, but also by changing the particle size. In order to study the effect of an enhanced electric field on a fluorophore, we used the DNA origami scaffold to position Cy3 in the gap between two AuNPs. We selected and extended two different sets of staple strands (three in each set), which are displayed from opposite faces of the origami plane (see SI Figures S32−S42 for detailed sequences of capture strands). The fluorophore-modified strand was the same for all assemblies examined. Cy3 has very similar emission and excitation maxima (550 nm excitation, and 565 emission) as that of TAMRA, as shown in Figure 5A. However, the intrinsic QE of Cy3 is 28%, significantly lower than that of TAMRA. For this reason, Cy3 is more likely to display QE enhancement. Figure 4 displays the schematic representation of the constructs in which the fluorophore is situated between the two AuNPs.

Photonic Interaction between Cy3 and 20 nm AuNP Dimer. We designed six different AuNP dimer constructs with three different interparticle distances (surface to surface): ~ 23 nm, ~ 40 nm, and ~58 nm for the 20 nm AuNPs, and ~20 nm, ~ 35 nm, and ~52 nm for the 30 nm AuNPs. The AuNPs are located on opposite faces of the 2D DNA origami structure to ensure that the dye molecule is positioned in the center between the two NPs. The constructs were purified using agarose gel electrophoresis and characterized by TEM after purification (see SI Figures S13−S18 for additional zoom out and zoom in images). It is apparent from the TEM images that the formation yield of the dimer after the purification is 90−95% (Figure 4A−C; see SI Table S2 for detailed statistical analysis). In the images, the interparticle gap generally appears smaller than the designed gap. This can be attributed to the fact that the underlying DNA origami scaffolds, when deposited on the surface of a TEM grid, are expected to adhere to the surface of the grid causing distortion of the DNA structure, especially when the AuNPs are located on opposite faces of the origami. When they are viewed from the top in the images (rather than from the side), this will decrease the apparent interparticle distance. In addition, drying the sample and the vacuum conditions used during TEM imaging can cause the structures to shrink. Fortunately, the interparticle distance should not be effected in aqueous solution, which is the condition used for all optical measurements. The interparticle distances reported here are based on the design, and consequently on the predictable structural characteristics of DNA structures. The uncertainty in the interparticle distance is limited by the distribution of AuNP diameters, rather than the structural uncertainty of DNA hybridization.

The high yield of assembled structures enables us to investigate the effect of an enhanced electric field on the fluorescence of Cy3 using the same bulk measurements that were used to examine the monomeric AuNP−dye arrangements. We initially performed the steady state fluorescence measurements of the 20 nm AuNP dimer samples and the corresponding control samples with excitation at 525 nm (Figure 5A; emission spectra shown in Figure S28). Figure 5B shows the ratio of the fluorescence intensity of the assembled sample and the control at the emission maximum, 565 nm. We observed very little quenching (~ 9%) for the construct with a large gap (58 nm) between AuNPs, and significantly higher quenching (38%) for 40 nm gap dimeric construct. Interestingly, when the gap between the particles was decreased to 23 nm, the ratio of fluorescence intensities was ~1, comparable with the control. These results are plotted in Figure 5B together with the theoretical simulations, which are in good agreement with experimental data. Remarkably, at very small gap distances, the data seems to reflect a perpendicular orientation of the dye with respect to the AuNP surface. This suggests that the internally labeled Cy3 has a fixed dipole moment along the DNA backbone.[32] When the dye-labeled DNA strand binds to the DNA origami structure, the orientation of the dye likely adopts an orientation nearly parallel to the central line of the AuNP dimer. The relative orientation changes as the positions of the AuNPs are adjusted (with the dye position held constant), which may explain the gradual change of the data points from closer to perpendicular to closer to the average orientation as the interparticle distance is adjusted.

We also performed TCSPC measurements of the fluorophore emission for the individual dimer constructs. The average lifetimes were calculated in the same way as previously described. The lifetime decay curves of the individual 20 nm AuNP constructs are plotted in Figure 5C. The average lifetime of Cy3-modified dsDNA is ~1.3 ns. For the AuNP dimer constructs with 58 and 40 nm gaps, the average lifetimes were shortened to ~1.00 ns and ~0.75 ns, respectively; the dimer with a 23 nm gap experienced a dramatic reduction in the

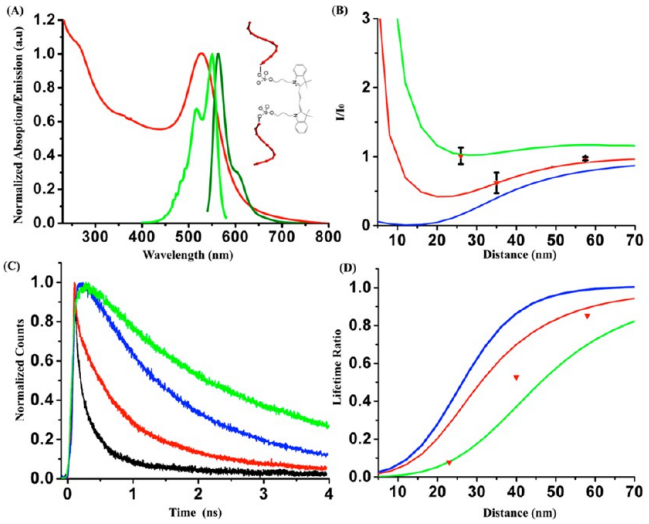

Figure 5. (A) Excitation (green) and emission spectra (olive) of Cy3 on dsDNA plotted with the AuNP plasmon band (red). Inset: Structure of an internally Cy3 modified DNA single strand. The dsDNA is formed by hybridization with the complementrary nonlabeled strand. (B) The fluorescence intensity ratios of the assembled sample to the control of 20 nm AuNP dimers (excitation at 525 nm and emission at 565 nm) for both interparticle distances are plotted with the theoretical predictions for different orientations of the dye with respect to the particle: average orientation (red), perpendicular orientation (green) and parallel orientation (blue). (C) Fluorescence lifetime decay curves corresponding to 20 nm AuNPs for different distances from Cy3 labeled dsDNA (green), 58 nm gap (blue), 40 nm gap (red) and 23 nm gap (black). (D) The average fluorescence lifetime ratio of the assembled sample to the control for different interparticle distances is plotted with the theoretical predictions for different orientations of the dye: average orientation (red), perpendicular orientation (green), and parallel orientation (blue).

average lifetime to ~0.11 ns. The ratios of the lifetimes of the assembled structures to the Cy3-labeled dsDNA versus the interparticle distance are plotted together with the simulated lifetime ratio in Figure 5D. The experimental data are in good agreement with the theoretical predictions.

Photonic Interaction between Cy3 and 30 nm AuNP Dimer. To evaluate the effect of more intense electric fields on the fluorescence of Cy3, we created AuNP dimer constructs from larger (30 nm) AuNPs. The 30 nm AuNP dimer−Cy3 dye structures were constructed with three different interparticle distances (20, 35, and 52 nm), characterized by TEM (Figure 4D−F; see SI Figures S19−S24 for more zoom-out and zoom-in TEM images), which exhibited excellent assembly yields (~90%) (see SI Table S2 for statistical details). In the TEM images, the interparticle gap appears smaller than the designed gap for the same reasons previously mentioned. We subsequently collected steady state and lifetime fluorescence measurements. Figure 6A shows the emission spectra of both 30 nm dimeric constructs excited at 525 nm. The emission spectra revealed that Cy3 QE is ~30% enhanced for the 52 nm interparticle distance and ~50% enhanced for the 20 and 35 nm interparticle distances. Figure 6B depicts the ratio of fluorescence intensity from the assembled sample to the corresponding control, plotted together with the theoretical prediction. The observed results are in agreement with the theory that predicts a mild enhancement of the QE for the range of interparticle distances examined in these experiments.

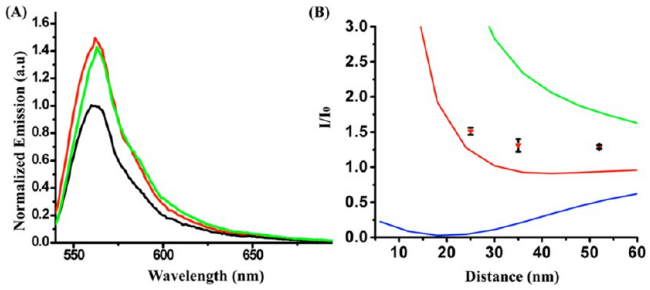

Figure 6. (A) Normalized fluorescence emission spectra (excited at 525 nm) of 30 nm dimeric structures with 20 nm gap (red) and 35 nm gap (green) with respect to the control (black). (B) The ratios of the fluorescence intensity at 565 nm for the assembled sample of the 30 nm AuNP dimers of different interparticle distances to the corresponding controls are plotted, together with the theoretical predictions for the differnet orientations of the dye with respect to the surface of the particles: average orientation (red), perpendicular orientation (green), and parallel orientation (blue).

All the data collected here falls between the curves corresponding to a perpendicular and an average orientation. The TCSPC meaurements did not yield reliable information about the fluorescence lifetimes as the decay was shortened below the time resolution of the instrument (response time of ~60 ps). Nevertheless, the measurements suggested very short lifetimes, as predicted by the theory described in Figure S29.

4. CONCLUSION

In summary, we used DNA origami as a molecular scaffold and nanoscale ruler to coassemble metallic NPs together with organic fluorophores and studied the corresponding distance-dependent photonic interations. Steady-state and lifetime measurements revealed that as the distance between a single AuNP and dye decreases, there is a corresponding increase in fluorescence quenching. The steady state and lifetime measurements also indicate that a higher nonradiative rate enhancement at smaller interparticle distances leads to the observed increase in fluorescent quenching. Rigorous electrodynamic calculations were performed, and the resulting predictions and existing empirical models are in agreement with our experimental observations. We also evaluated the effect of relatively stronger electric fields on the fluorescence of an organic dye. In order to do so, we constructed dimeric AuNP structures with different interparticle distances and positioned a dye with lower QE in the gap between the particles. For dimeric 30 nm AuNP−dye structures, we observed 50% enhancement in the QE of the dye for shorter distances. These results are supported by theoretical simulations. The observed enhancement is accompanied by a significantly faster fluorescence decay rate, indicating a greater enhancement of the radiative decay rate than the nonradiative decay rate.

The DNA-directed self-assembly method utilized here could be used to construct NP assemblies that exhibit very high electric field enhancements. For example, dimers of gold or silver nanorods could lead to much higher enhancements in the fluorescence of organic dyes or photoemission of quantum dots. Single molecule evaluation of these structures, with incredibly high assembly yields and precisely controlled interparticle distance, will ensure reliable observation of the photonic interactions between NPs and fluorophores or quantum dots.

dx.doi.org/10.1021/jp312422n | J. Phys. Chem. C 2013, 117, 12735−12744

■ ASSOCIATED CONTENT

Supporting Information

Methods for the steady state and dynamic fluorescence measurements, equations used in the calculations, additional TEM images, yield analysis, original data of emission spectra and decay, dye−particle distance calculation, and DNA sequences are included in the SI. This information is available free of charge via the Internet at http://pubs.acs.org.

■ AUTHOR INFORMATION

Corresponding Author

*Telephone: 480-727-0397; E-mail: yan_liu@asu.edu.

Notes

The authors declare no competing financial interest.

■ ACKNOWLEDGMENTS

This research was partly supported by grants from the ONR, ARO, and NSF to Y.L., from the ONR, ARO, NSF, and Sloan Research Foundation to H.Y., and from the ONR, NSF, and ACS/PRF to S.Z. The authors acknowledge the use of the EM facility in School of Life Science at Arizona State University. We thank Dr. Su Lin and Dr. Gerdenis Kodis for the help in lifetime measurements and stimulating discussions. We thank Dr. Jeanette Nangreave for proofreading the text.

■ REFERENCES

(1) Aldaye, F. A.; Palmer, A. L.; Sleiman, H. F. Assembling Materials with DNA as a Guide. *Science* **2008**, *321*, 1795−1799.

(2) Rothemund, P. W. K. Folding DNA to Create Nanoscale Shapes and Patterns. *Nature* **2006**, *440*, 297−302.

(3) Ke, Y.; Douglas, S. M.; Liu, M.; Sharma, J.; Cheng, A.; Leung, A.; Liu, Y.; Shih, W. M.; Yan, H. Multilayer DNA Origami Packed on a Square Lattice. *J. Am. Chem. Soc.* **2009**, *131*, 15903−15908.

(4) Han, D.; Pal, S.; Liu, Y.; Yan, H. Folding and Cutting DNA into Reconfigurable Topological Nanostructures. *Nat. Nanotechnol.* **2010**, *5*, 712−717.

(5) Deng, Z. T.; Samanta, A.; Nangreave, J.; Yan, H.; Liu, Y. Robust DNA Functionalized Core/Shell Quantum Dots with Fluorescent Emission Spanning from UV−Vis to Near-IR and Compatible with DNA Directed Self-Assembly. *J. Am. Chem. Soc.* **2012**, *134* (42), 17424−17427.

(6) Maune, H. T.; Han, S.-p.; Barish, R. D.; Bockrath, M.; Goddard, W. A., III; Rothemund, P. W. K.; Winfree, E. Self-Assembly of Carbon Nanotubes into Two-Dimensional Geometries Using DNA Origami Templates. *Nat. Nanotechnol.* **2009**, *4*, 61−66.

(7) Stephanopoulos, N.; Liu, M.; Tong, G. J.; Li, Z.; Liu, Y.; Yan, H.; Francis, M. B. Immobilization and One-Dimensional Arrangement of Virus Capsids with Nanoscale Precision Using DNA Origami. *Nano Lett.* **2010**, *10*, 2714−2720.

(8) B Sacca, B.; Meyer, R.; Erkelenz, M.; Kiko, K.; Arndt, A.; Schroeder, H.; Rabe, K. S.; Niemeyer, C. M. Orthogonal Protein Decoration of DNA Origami. *Angew. Chem., Int. Ed.* **2010**, *49*, 9378−9383.

(9) Chhabra, R.; Sharma, J.; Ke, Y.; Liu, Y.; Rinker, S.; Lindsay, S.; Yan, H. Spatially Addressable Multiprotein Nanoarrays Templated by Aptamer-Tagged DNA Nanoarchitectures. *J. Am. Chem. Soc.* **2007**, *129*, 10304−10305.

(10) Rinker, S.; Ke, Y.; Liu, Y.; Chhabra, R.; Yan, H. Assembled DNA Nanostructures for Distance-Dependent Multivalent Ligand−Protein Binding. *Nat. Nanotechnol.* **2008**, *3*, 418−422.

(11) Fu, J. L.; Liu, M. H.; Liu, Y.; Woodbury, N. W.; Yan, H. Interenzyme Substrate Diffusion for an Enzyme Cascade Organized on Spatially Addressable DNA Nanostructures. *J. Am. Chem. Soc.* **2012**, *134*, 5516−5519.

(12) Sharma, J.; Chhabra, R.; Andersen, C. S.; Gothelf, K. V.; Yan, H.; Liu, Y. Toward Reliable Gold Nanoparticle Patterning on Self-Assembled DNA Nanoscaffold. *J. Am. Chem. Soc.* **2008**, *130*, 7820−7821.

(13) Ding, B.; Deng, Z. T.; Yan, H.; Cabrini, S.; Zuckermann, R. N.; Bokor, J. Gold Nanoparticle Self-Similar Chain Structure Organized by DNA Origami. *J. Am. Chem. Soc.* **2010**, *132*, 3248−3249.

(14) Hung, A. M.; Micheel, C. M.; Bozano, L. D.; Osterbur, L. W.; Wallraff, G. M.; Cha, J. N. Large-Area Spatially Ordered Arrays of Gold Nanoparticles Directed by Lithographically Confined DNA Origami. *Nat. Nanotechnol.* **2010**, *5*, 121−126.

(15) Pal, S.; Varghese, R.; Deng, Z. T.; Zhao, Z.; Kumar, A.; Yan, H.; Liu, Y. Site-Specific Synthesis and In Situ Immobilization of Fluorescent Silver Nanoclusters on DNA Nanoscaffolds by Use of the Tollens Reaction. *Angew. Chem., Int. Ed.* **2011**, *50*, 4176−4179.

(16) Zhao, Z.; Jacovetty, E. L.; Liu, Y.; Yan, H. Encapsulation of Gold Nanoparticles in a DNA Origami Cage. *Angew. Chem., Int. Ed.* **2011**, *50*, 2041−2044.

(17) Pal, S.; Deng, Z. T; Ding, B.; Yan, H.; Liu, Y. DNA-Origami-Directed Self-Assembly of Discrete Silver-Nanoparticle Architectures. *Angew. Chem., Int. Ed.* **2010**, *49*, 2700−2704.

(18) Pal, S.; Deng, Z. T; Wang, H.; Zou, S.; Liu, Y.; Yan, H. DNA Directed Self-Assembly of Anisotropic Plasmonic Nanostructures. *J. Am. Chem. Soc.* **2011**, *133*, 17606−17609.

(19) Stewart, M. E.; Anderton, C. R.; Thompson, L. B.; Maria, J.; Gray, S. K.; Rogers, J. A.; Nuzzo, R. G. . Nanostructured Plasmonic Sensors. *Chem. Rev.* **2008**, *108*, 494−521.

(20) Shen, X. B.; Song, C.; Wang, J. Y.; Shi, D. W.; Wang, Z. A.; Liu, N.; Ding, B. Q. Rolling up Gold Nanoparticle-Dressed DNA Origami into Three-Dimensional Plasmonic Chiral Nanostructures. *J. Am. Chem. Soc.* **2012**, *134*, 146−149.

(21) Kuzyk, A.; Schreiber, R.; Fan, Z.; Pardatscher, G.; Roller, E.; Högele, A.; Simmel, F.; Govorov, A. O.; Liedl, T. DNA-Based Self-Assembly of Chiral Plasmonic Nanostructures with Tailored Optical Response. *Nature* **2012**, *483*, 311−314.

(22) Chhabra, R.; Sharma, J.; Wang, H. N.; Zou, S. L.; Lin, S.; Yan, H.; Lindsay, S.; Liu, Y. Distance-Dependent Interactions Between Gold Nanoparticles and Fluorescent Molecules with DNA as Tunable Spacers. *Nanotechnology* **2009**, *20*, 485201−485201.

(23) Yun, C. S.; Javier, A.; Jennings, T.; Fisher, M.; Hira, S.; Peterson, S.; Hopkins, B.; Reich, N. O.; Strouse, G. F. Nanometal Surface Energy Transfer in Optical Rulers, Breaking the FRET Barrier. *J. Am. Chem. Soc.* **2005**, *127*, 3115−3119.

(24) Capehart, S. L.; Coyle, M. P.; Glasgow, J. E.; Francis, M. B. Controlled Integration of Gold Nanoparticles and Organic Fluorophores Using Synthetically Modified MS2 Viral Capsids. *J. Am. Chem. Soc.* **2013**, *135*, 3011−3016.

(25) Acuna, G. P.; Bucher, M.; Stein, I. H.; Steinhauer, C.; Kuzyk, A.; Holzmeister, P.; Schreiber, R.; Moroz, A.; Stefani, F. D.; Liedl, T.; et al. Distance Dependence of Single-Fluorophore Quenching by Gold Nanoparticles Studied on DNA Origami. *ACS Nano* **2012**, *6*, 3189−3195.

(26) Liu, X.; Atwater, M.; Wang, J.; Huo, Q. Extinction Coefficient of Gold Nanoparticles with Different Sizes and Different Capping Ligands. *Colloids Surf. B* **2007**, *58*, 3−7.

(27) Lakowicz, J. R. *Principles of Fluorescence Spectroscopy*, 2nd ed.; Kluwer Academic Plenum: New York, 1999.

(28) Zou, S.; Schatz, G. C. Silver Nanoparticle Array Structures that Produce Giant Enhancements in Electromagnetic Fields. *Chem. Phys. Lett.* **2005**, *403*, 62−67.

(29) Zou, S.; Schatz, G. C. Metal Nanoparticle Array Waveguides: Proposed Structures for Subwavelength Devices. *Phys. Rev. B* **2006**, *74*, 125111(1−5).

(30) Novotny, L.; van Hulst, N. Antennas for Light. *Nat. Photonics* **2011**, *5*, 83−90.

(31) Busson, M. P.; Rolly, B.; Stout, B.; Bonod, N.; Bidault, S. Accelerated Single Photon Emission from Dye Molecule-Driven Nanoantennas Assembled on DNA. *Nat. Commun.* **2012**, *3*, 962.

(32) Ranjit, S.; Gurunathan, K.; Levitus, M. Photophysics of Backbone Fluorescent DNA Modifications: Reducing Uncertainties in FRET. *J. Phys. Chem. B* **2009**, *113*, 7861−7866.

(33) Chance, R. R.; Prock, A.; Silbey, R. Molecular Fluorescence and Energy Transfer Near Interfaces. *Adv. Chem. Phys.* **1978**, *37*, 1−65.
(34) Gersten, J. I.; Nitzan, A. Spectroscopic Properties of Molecules with Small Dielectric Particles. *J. Chem. Phys.* **1981**, *75*, 1139−1152.